Liquid-Glassy Polymer Diffusion: Effects of Liquid Molecular Weight and Temperature

J. Pablo Tomba,* Luis M. Arzondo, José M. Carella, José M. Pastor

We examine mechanistic aspects of the diffusion between a series of liquid polystyrenes (PS) and a glassy poly(phenylene oxide) (PPO) matrix, through the use of confocal Raman microspectroscopy. The results show that the diffusion kinetics has Fickean characteristics, similar to those found in liquid-liquid polymer diffusion. No signatures of the linear regime typical of the case-II diffusion mechanism were found. Overall, these observations are consistent with the claim that case-II is unlikely to occur in liquid-glassy polymer diffusion.

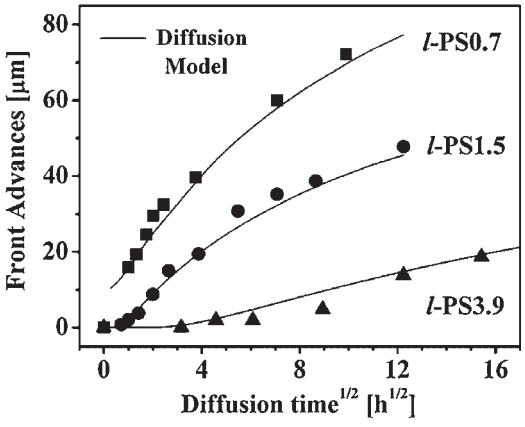

Introduction

Polymer diffusion governs a number of important dynamic processes such as adhesion, phase separation, and mixing. In parallel to the classic situation where diffusion occurs between two polymers in the melt state, wide attention has been paid to those interphases involving one of the polymers in the glassy state. It gives rise to a case of liquid-glassy polymer diffusion, as can be found in numerous fields of technology such as membranes for separation technologies, packing and coatings, polymer blends with hard and soft components, systems for controlled drug delivery, and lithography in microelectronics among others.

The principles that govern interphase evolution in polymer melts are well understood. On the scale where end-to-end distances of a small section of the chains are nearly Gaussian, Rouse modes are the natural basis for chain dynamics, usually described in terms of a friction coefficient associated with the monomeric unit.[1] At larger lengths and longer time scales, chain dynamics is strongly influenced by entanglements. In this case, the reptation model developed by de Gennes, which envisions a Rouse chain moving along a tube defined by the other chains, is used to describe the interphase kinetics.[2] The same principles apply to polymer blends in the melt state. In composition regimes where the amounts of the constituent polymers are nearly balanced, thermodynamic interactions play an important role.[3] In polymer blends with components that differ in their glass transition temperatures (T_g), the monomer friction coefficients of the individual components can differ by several decades at the temperature of the experiment, leading to a marked

J. P. Tomba, J. M. Carella
Institute of Materials Science and Technology (INTEMA), National Research Council (CONICET), University of Mar del Plata, Juan B. Justo 4302, 7600 Mar del Plata, Argentina
E-mail: jptomba@fi.mdp.edu.ar
L. M. Arzondo
Department of Industrial Engineering, UTN, Faculty of Río Grande, Islas Malvinas 1650, 9420 Río Grande, Argentina
J. M. Pastor
Department of Physics of Condensed Matter, University of Valladolid, Paseo del Cauce s/n, 47011 Valladolid, Spain

Macromol. Chem. Phys. 2007, 208, 1110–1121

DOI: 10.1002/macp.200600658

asymmetry in the distribution of compositions at the interphase.[4,5] The aspects discussed above have been quantitatively described in such a way that interphase dynamics can be successfully predicted in terms of Fick's diffusion equations, regardless of the fact that some issues, such as the distinctive chain dynamics that each component may exhibit in the polymer blend and its resulting thermorheological complex behavior, still require a deeper comprehension.[6]

In contrast, our understanding of how the interphase evolves in systems comprising one of the polymers in the glassy state is more limited and in many cases diffusion deviates from the Fickian behavior. For example, it is well established that, in certain conditions, the penetration and diffusion of small-sized molecules in glassy polymers follows the case II diffusion mechanism. In this remarkable non-Fickian diffusion process, interphase evolution is controlled by the mechanical relaxation of the glassy polymer, as proposed in the seminal work of Thomas and Windle,[7] later confirmed by Kramer.[8,9] In a typical experiment, a glassy polymer is placed in contact with the source of small-sized molecules in the liquid state. Driven by osmotic suction,[10] the highly mobile small molecules penetrate into the glassy matrix forming a Fickian tail, considerably swelling the polymer layer that can still remain in the glassy state. The swollen polymer generates stresses in the adjacent non-swollen glassy matrix of the order of its yield stress. Case II diffusion operates when the induced stress effectively overcomes the deformation resistance of the glassy matrix. At this point, further penetration of the small molecules is controlled by the time-dependent mechanical response of the glassy polymer. The nature of this rate-controlling step explains the characteristic linear sorption kinetics typically reported in case II, markedly different to that observed in Fickian diffusion.

Whether these unique features observed in the case of small molecules can be extended to the case of larger molecules, i.e., oligomers and polymers with moderate molecular weight above their glass transition temperature, is a topic that remains on debate, as shown by many recent work published on this subject.[11–16] One group of authors has extended the concept of case II to explain the characteristics of the liquid/glassy polymer diffusion.[14,17,18] The more solid argument in favor of a mechanism of diffusion controlled by the mechanical relaxation of the solid matrix has been the characteristic shape of the concentration profiles of the liquid polymer, that closely resemble those observed in case II. These ideas have been questioned by other group of authors, who have suggested that the growth mechanism for these interphases may be diffusion controlled, similar to that observed in liquid-liquid polymer diffusion between species with different physical properties.[13,15] The main argument against case II in these cases has been pointed toward the extremely low osmotic suction values associated with the large polymer molecules, insufficient to trigger the mechanism of mechanically controlled liquid penetration described above.[16]

The polystyrene (PS)-poly(phenylene oxide) (PPO) polymer pair is an ideal system to test these ideas. Both components have very different T_g and a well-characterized blend dynamics in the melt state.[4] Significantly, the reports on the operating mechanism in diffusion experiments between liquid-PS and glassy-PPO have been contradictory.[14,19] Our goal in this work was to focus on those specific aspects of the problem that may help to elucidate the diffusion control mechanism in this polymer pair. We expanded the range of molecular weights of the liquid component in the lower end, which, conceivably, might allow us to observe a range of effects. On one hand, lower liquid molecular weights are associated with larger values of osmotic suction, a favorable condition for case II. As osmotic suction can be tuned by varying liquid molecular weight, we explore for possible changes in the diffusion control mechanism with liquid molecular weight. On the other hand, the use of liquid polymers in the range of molecular weights where chain ends play a role ought to affect sensitively the kinetics of a liquid interphase, as predicted by well-established theories on polymer melts. In parallel, we pay special attention to the effect of temperature on the diffusion process, bearing in mind that the response to this parameter is expected to be markedly different for case II and Fickian diffusion.[7] Finally, the experiments were carried out at temperatures well below and in the vicinity of the PPO-rich matrix T_g to directly compare diffusion rates with the liquid-liquid polymer diffusion case. To monitor polymer diffusion, we employed a combination of optical and physical sectioning with confocal Raman microspectroscopy (CRM), an experimental technique that allows direct mapping of interphase composition and its temporal evolution.

Experimental Part

Materials Characterization

The nearly monodisperse ($\overline{M}_w/\overline{M}_n = 1.05$) PS samples were purchased from Polymer Source (Dorval, Canada). These samples are referred to here as PS0.7 ($\overline{M}_w = 740\ g \cdot mol^{-1}$, $T_g = -5\ ^\circ C$), PS1.5 ($\overline{M}_w = 1\,460\ g \cdot mol^{-1}$, $T_g = 45\ ^\circ C$), and PS3.9 ($\overline{M}_w = 3\,900\ g \cdot mol^{-1}$, $T_g = 77\ ^\circ C$). The PPO sample ($\overline{M}_n = 31\,000\ g \cdot mol^{-1}$, $\overline{M}_w/\overline{M}_n = 2.0$, $T_g = 212\ ^\circ C$) was purchased from Aldrich. Details of the molecular weight characterization were provided by the manufacturer. Glass transition temperatures for pure polymers and for PS-PPO blends were measured by DSC on a Perkin-Elmer Pyris II DSC instrument. Samples were first cooled and later heated from $-25\ ^\circ C$ at a rate of $10\ ^\circ C \cdot min^{-1}$ under N_2 atmosphere. Glass transition temperatures were determined as the onset of the transition.

Table 1. Characteristics of the samples used for diffusion experiments.

System	Low-T_g layer		High-T_g layer		Diffusion temperatures
	Φ^{PS}	T_g	Φ^{PS}	T_g	°C
		°C		°C	
l-PS0.7/PPO	0.7	25	0.05	200	120, 140, 160, 180
l-PS1.5/PPO	0.9	51	0.1	182	140, 160, 180, 200
l-PS3.9/PPO	0.9	80	0.1	185	160, 180, 200, 220

Sample Preparation for Diffusion Experiments

Details of the samples used for the whole set of diffusion experiments, including layer compositions, layer thicknesses and diffusion temperatures, are given in Table 1. PS-PPO blends for the bilayer samples used for diffusion experiments were prepared by freeze drying of benzene solutions of about 10 wt.-%. Antioxidant (100 ppm, Santonox, Ciba-Geigy) was added to the blends to prevent oxidation. The blends were annealed overnight under vacuum at temperatures above T_g, prior to the molding step, to exhaustively remove any trace of solvent. Solvent removal was verified by checking for lack of T_g changes by DSC.

Composite plates for diffusion experiments were prepared by sequential vacuum molding of a PPO-rich thick layer (500 μm thick) and a PS-rich thinner layer (50–100 μm thick), in the form of cylindrical specimens (20 mm diameter). Details of the molding protocol and the apparatus used can be found elsewhere.[19] The thick layer was first vacuum molded at temperatures at least 20 °C above its T_g, using a set of cylindrical molds and sliding pistons, as detailed previously.[19] The surface of the thick glassy layer observed under optical microscope looked essentially flat. The thinner layer was then vacuum molded on top of this layer, at temperatures 20 K above its T_g, and well below the thick layer T_g, for a short period of time (15 min), to minimize diffusion at this stage.

Diffusion between layers of the composite plates was promoted by annealing for specified times in a temperature-controlled oven (±0.5 °C). The oven was continuously flushed with dry nitrogen, to avoid oxidation of the samples. The samples were periodically removed from the oven for diffusion measurements and were allowed to quickly cool back to room temperature, which virtually stops polymer diffusion, before Raman measurements were performed.

Confocal Raman Microspectroscopy

Local Raman spectra were measured at room temperature on a microspectrometer DILOR LabRam Confocal, equipped with a 16-mW He-Ne laser beam (632.8 nm wavelength). In the excitation and collection path, an Olympus x100 (NA = 0.9) objective was used. A slit opening of 500 μm and a holographic grating of 1 800 lines · mm^{-1} were used which allowed data acquisition in a Raman shifts range of 500–1 500 cm^{-1} with a spectral resolution of 5 cm^{-1}. The acquisition time for each spectrum varied between 20–45 s and 5–10 spectra were accumulated for each data point.

Optical sectioning by depth profiling was carried out as explained in earlier work.[19] The laser beam is focused on the outer surface of the thin PS-rich layer, and then at successively deeper positions into the sample and across the PS/PPO interphase. In this way, interphase evolution can be monitored in a given sample spot without altering the specimen. The nominal depth resolution in our working conditions (pinhole opening between 100 and 300 μm) is 5 μm, as determined by measuring the instrumental response in normal direction to a polished silicon wafer, a routine test in CRM. Due to laser refraction, this value progressively increases as we focus deeper into the sample; a detailed description of this phenomenon can be found elsewhere.[19,20] The depth scale was properly corrected for refraction distortions as explained in earlier work.[19] Surface profiling by CRM renders superior and invariant spatial resolution, but, as a disadvantage, it is destructive. The technique requires physical sectioning of the sample to directly expose the interphase to the laser beam. Sample microtoming was carried out at room temperature in a Leica microtome (model RM2055). The liquid-PS diffusion path was then scanned by focusing the microscope objective perpendicular to the diffusion direction.[21] The lateral dimension of the laser probe was about 1 μm, as obtained by scanning laterally a piece of silicon. For each diffusion time, the concentration profile was measured by taking several Raman spectra at different points along the diffusion path, in steps of 2–5 μm (typically 30–40 measurements). Local chemical compositions were calculated from the acquired Raman spectra with the linear decomposition method and a calibration curve relating concentration with Raman intensity.[22]

Results and Discussion

Diffusion Profiles of the Liquid Polymers

We examine first the effect of the physical state of the matrix and the liquid PS molecular weight on the shape of the liquid-diffusion profiles. A family of diffusion profiles in a form of liquid-PS concentration versus depth is shown through Figure 1(a)–1(c). To obtain the profiles, the optical sectioning by confocal Raman was started at the outer surface of the PS-rich layer, the zero in the depth scale axis, and then repeated at deeper positions along the PS diffusion path. Figure 1(a) shows the volume fraction of PS0.7 at the PS/PPO interphase for a sample annealed at 140 °C, well below the matrix T_g (200 °C), for several diffusion times. Figure 1(b) shows data for a sample containing PS1.5, annealed at 160 °C, in the proximity of the matrix T_g (182 °C). Figure 1(c) corresponds to diffusion experiments with the sample containing PS3.9, annealed at 200 °C, 15 °C above the matrix T_g (185 °C).

The liquid-PS profiles look similar, independently of the physical state of the matrix, either as a glassy solid [Figure 1(a)] or a viscous liquid [Figure 1(c)]. The shape of

Macromolecular Journals
DOI: 10.1002/macp.200600658

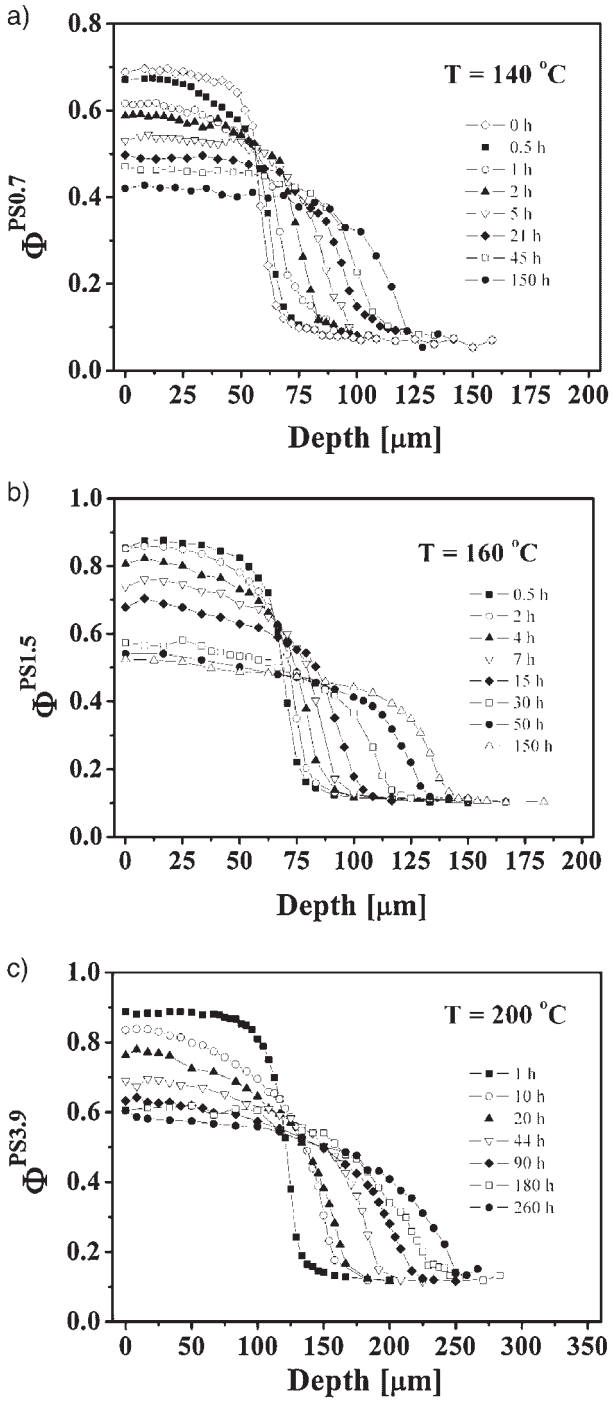

Figure 1. Typical liquid PS concentration profiles obtained by confocal Raman depth profiling for the systems studied: (a) *l*-PS0.7/PPO at 140 °C; (b) *l*-PS1.5/PPO at 160 °C; and (c) *l*-PS3.9/PPO at 200 °C. The diffusion times are indicated in the plot.

the profiles is also independent of the liquid molecular weight. As a common feature in these experiments, the limited supply of liquid-PS advances toward the glassy PPO-rich layer as time increases. Moving along the PS diffusion path, the PS concentration profiles are at first fairly flat along the outer 50–75 μm (plateau region). Then, their slope becomes increasingly higher and the PS concentration decreases rapidly, reaching the levels corresponding to the PPO-rich layer. The limited PS supply causes the PS concentration at the plateau region to decrease with diffusion time.

In our experiments, the transition from the liquid PS-rich region to the glassy PPO-rich layer appears smoothed and artificially extended over a region of tens of microns on the depth scale, due to limitations in the spatial resolution of the depth-profiling confocal Raman technique. To demonstrate that the blurring is merely instrumental, we carried out parallel experiments in which we profiled the interphase employing surface analysis, a focusing technique with superior spatial resolution. A different set of samples were subjected to the same annealing conditions, and, after pre-established annealing times, physically cut along a plane parallel to the PS diffusion path, to perform the surface analysis (see Experimental Part). Figure 2(a)–2(c) show selected examples of PS/PPO interphases probed on a finer scale for experiments carried out at temperatures well below, within, and above the matrix T_g. The *x*-axis of these plots has been labeled as spatial coordinate instead of depth, to emphasize the fact that these data were not obtained by depth profiling. The symbols correspond to experimental data while the continuous lines correspond to model predictions that will be discussed below.

Observed at higher spatial resolution the PS profiles of Figure 2(a)–2(c) still look similar, independent of temperature and liquid molecular weight. The transition from the PS-rich to the PPO-rich layer is actually abrupt and occurs over a narrow range on the depth scale (1–2 μm), in the form of sharp diffusion front. No leading tails of liquid-PS in the PPO-rich phase can be seen in the scale of the lateral resolution of the micro-Raman technique, about 1 μm.

The presence of tails is particularly relevant from the perspective of the case II mechanism, where the small liquid molecules form a Fickian footstep preceding the advancing diffusion front. This Fickian precursor plays an important role in plasticizing and swelling the glassy matrix, additionally reducing its yield stress. The precursor is produced by a very low concentration of the small molecules that fill interstitial sites in the glassy polymer (free volume), with a diffusion kinetics very sensitive to the effective cross-section of the small molecule, which in turns depends on its shape and molecular weight.[9b] One would expect that the probability that local fluctuations in density produce a hole of sufficient size for a large-sized molecule to move is very small. For example, for bromoalkanes with less than ten carbon atoms diffusing in solid PS, the Fickian precursors are typically in the range of several hundreds of nanometers, decreasing in extension as the number of carbon atoms increases.[9b]

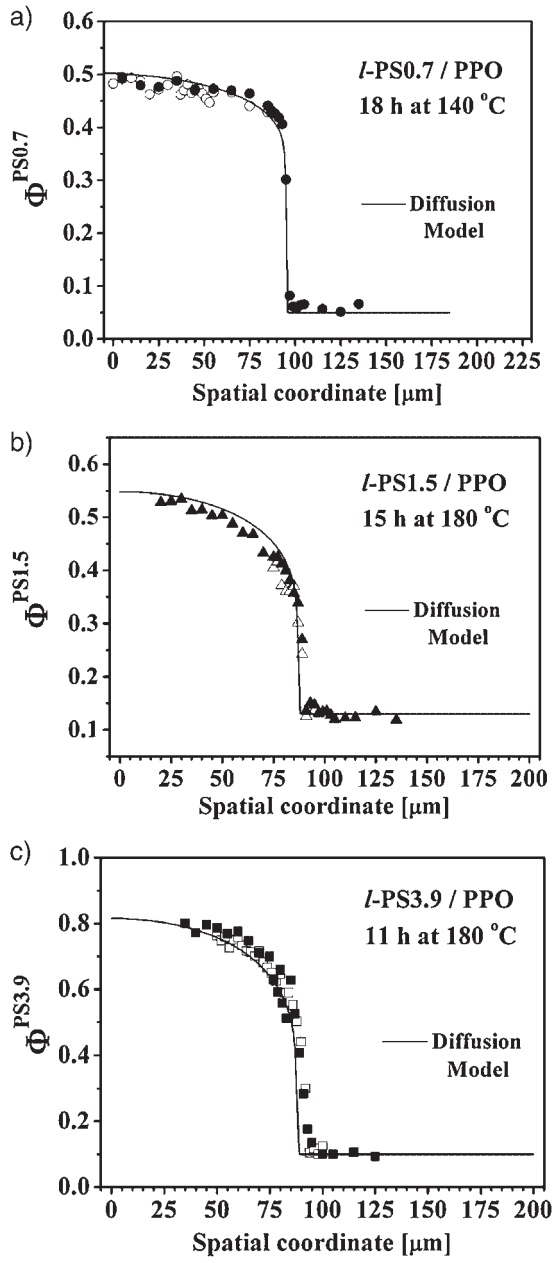

Figure 2. PS concentration profiles obtained by surface profiling with confocal Raman corresponding to: (a) *l*-PS0.7/PPO; (b) *l*-PS1.5/PPO; and (c) *l*-PS3.9/PPO; for the times and temperatures indicated in the plot. Solid lines correspond to model predictions.

Conversely, the Fickian precursors are absent in experiments involving high-molecular weight liquid penetrants such as polymers above T_g, as observed independently by Kramer[23] and Lin[14] in their studies on the diffusion of high molecular weight liquid PS in contact with glassy PPO. The chemical composition profiles of the high molecular weight liquid penetrants reported by these authors did not show noticeable tails inside the glassy polymer matrices, looking similar to those we reported in Figure 2(a)–2(c). Notice that the techniques employed by them, Rutherford backscattering spectrometry and secondary ions mass spectroscopy, have very high spatial resolution (few nanometers). Lin et al. reported[14] what they call "intermixing layer", a region at the glassy side of the liquid PS/glassy PPO interphase, where the PS concentration changes abruptly over a very short distance (about 30 nm), which might be seen at first glance as a Fickian tail. Nonetheless, the width of this layer is in the order of the average end-to-end distances of the PPO molecules,[24] which suggests that the observed changes in PS concentration cannot be ascribed to the center-of-mass diffusion described by the Fick's law. To explain the existence of this thin layer, we imagine that the sequence of events that give rise to the PPO transport starts when the PS molecules plasticize first the PPO molecules at the interface (almost one at a time), with Rouse-like movements that occur over a length scale smaller than the radius of gyration of the PPO molecules. Then, this is followed by the center-of-mass movements of the PPO molecules toward the PS-rich liquid layer in Fickian fashion. We believe that this picture, advanced earlier,[16] explains more satisfactory the experimental facts.

Interphase Kinetics and Effect of the Liquid PS Molecular Weight

Our analysis on diffusion kinetics focuses on the time evolution of the diffusion fronts and the plateau region behind. While the kinetics of the diffusion fronts reflects the relative speeds of the sequence of events that control the interphase progress, polymer mobility throughout the plateau region is the highest and its time evolution is very sensitive to the features that control the diffusion process. Although the time evolution of the average composition throughout the plateau region can be directly measured from the diffusion profile, the exact localization of the diffusion front in depth-profiling experiments is slightly trickier because of the before mentioned broadening due to instrumental artifacts. The procedure we have followed to calculate this parameter takes advantage of the almost rectangular shape of the real PS concentration profiles, as seen through Figure 2. Thus, we can directly calculate the PS advancing front positions into the glassy PPO-rich layer from the plateau concentration value and the area under the profile, required to be constant by mass conservation. This method, detailed in earlier work,[11,16] has been used here to obtain the time evolution of the front advances from the liquid profiles measured by depth profiling.

We next consider the influence of the molecular weight of the liquid polymer on the interphase kinetics. We begin by comparing the diffusion kinetics of the series of low molecular weight PS at a given annealing temperature, as

Macromol. Chem. Phys. **2007**, *208*, 1110–1121

Macromolecular Journals
DOI: 10.1002/macp.200600658

shown in Figure 3(a)–3(b). In Figure 3(a), we compare the successive front positions as a function of annealing time, to analyze the diffusion kinetics in the context of the case II diffusion theory. Figure 3(b) shows the same plot in Fickian fashion, as a function of the square root of the elapsed diffusion time. The data of both figures correspond to samples annealed at 160 °C, a temperature well below the T_g of any of the matrices. Figure 3 represents a common pattern observed in all the experiments: the displacement of the liquid PS diffusion fronts toward the PPO-rich matrix is always markedly nonlinear with time and there is no indication of change in the diffusion kinetics with the liquid molecular weight. We also observe that the diffusion front advances scale relatively better with $t^{1/2}$, although a departure in the form of a downward curvature is observed in all the cases at long diffusion times. The origin of this deviation in the context of Fickian diffusion along with the observed time-scaling laws will be further discussed below.

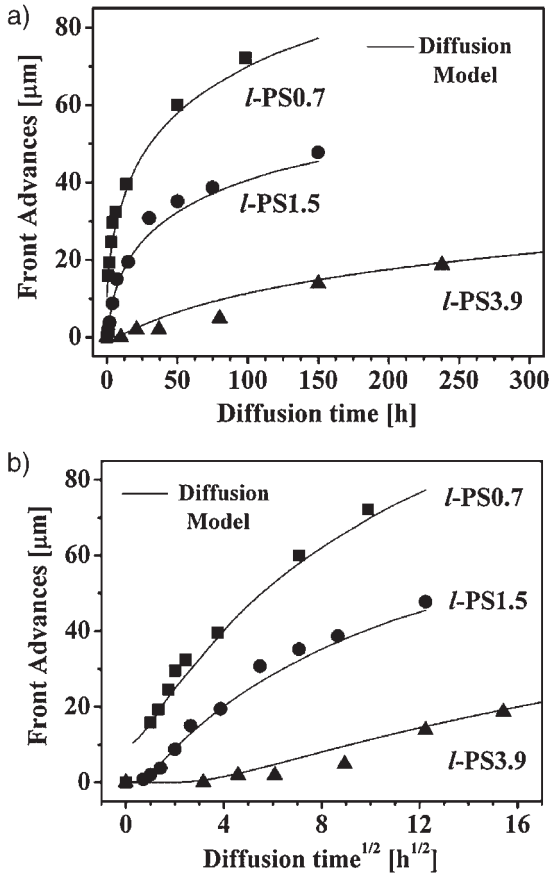

Figure 3. Kinetics of the advancing PS-liquid diffusion fronts for experiments carried out at 160 °C: (a) advances of the diffusion front as a function of the elapsed time and (b) as a function of the square root of the elapsed time. Symbols correspond to experimental data of the three systems examined; solid lines correspond to model predictions.

The data in Figure 3 also indicate that the molecular weight of the liquid polymer affects significantly the rate of polymer diffusion. In the series examined, the molecular weights are in a 1:2:5 PS0.7/PS1.5/PS3.9 ratio. Although the T_g of the solid matrices are comparable (200, 180, and 185 °C), the T_g of the polymer blends containing the liquid polymer are quite different (25, 51, and 80 °C). In the context of case II theory, the diffusion front velocity is related with the liquid molecular weight through the diffusion coefficients of the liquid penetrant in the solid matrix, and through the swelling rate, a parameter that depends very sensitively on the osmotic suction associated with the liquid and on its ability in plasticizing the glassy polymer.[9b] This rather complex dependence of the swelling rate with liquid molecular weight precludes a detailed calculation of front velocities as function of liquid molecular weight. In contrast, the prediction of front velocities in the context of polymer liquid dynamics, where the temperature interval with respect to T_g plays a central role, is accessible through existing data of the monomeric friction coefficients for the components as a function of temperature and composition. This issue will be addressed in the next sections.

Interphase Kinetics at Various Temperatures

In this section, we consider the influence of the physical state of the matrix on the diffusion kinetics, through changes in the diffusion temperature. Figure 4 shows the evolution of the liquid-PS concentration at the plateau region as a function of the diffusion time for the *l*-PS1.5/PPO pair, in a range of temperatures that encompasses the T_g of the glassy matrix (182 °C). The experimental data shown correspond to averaged values for the first 50 μm

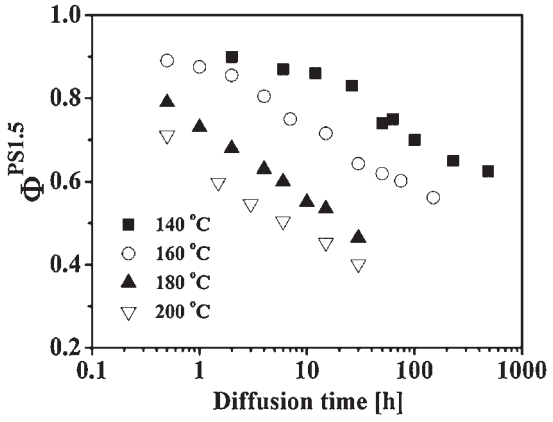

Figure 4. Chemical composition of the plateau region behind the advancing diffusion front (as PS volume fractions) as a function of the elapsed diffusion time for the *l*-PS1.5/PPO system. Each diffusion temperature is identified with a different symbol as indicated in the graph.

of the PS-rich layer and these have been represented using a different symbol for each diffusion temperature.

The slopes observed in each of these curves reflect the dependence of the parameters that control the diffusion process on composition or diffusion time. Remarkably, the data show the same trend for experiments performed below and above the matrix T_g, despite of the dramatic differences in the physical state of the PPO-rich matrix, suggesting that the rate-controlling step is outside the PPO-rich matrix. The absence of any indication of change in the diffusion behavior when passing thorough the matrix T_g was also observed in the *l*-PS0.7/PPO and *l*-PS3.9/PPO systems. This fact indicates that the parameters that control the *l*-PS diffusive transport and their dependence on composition are the same regardless of the physical state of the glassy polymer, as already observed in experiments carried out with the same philosophy on the PS/PVME system.[16]

In Figure 5, we plot advances of the diffusion fronts as a function of annealing time [Figure 5(a)] and in Fickian fashion [Figure 5(b)] for the *l*-PS0.7 and *l*-PS1.5 systems. The plots include data from experiments carried out well below and in the vicinity of the glassy matrix T_g.

We observe the already mentioned nonlinear displacement of the liquid PS diffusion fronts in the PPO-rich matrix, which clearly appears as a common characteristic of our experiments. This fact is not surprising for the experiments conducted above the T_g of the glassy matrix [curve at 200 °C for the *l*-PS1.5 system in Figure 5(a)], for which polymer diffusion is known to be Fickian. However, the marked deviation of the front positions from a linear scaling law observed in experiments below the T_g of the

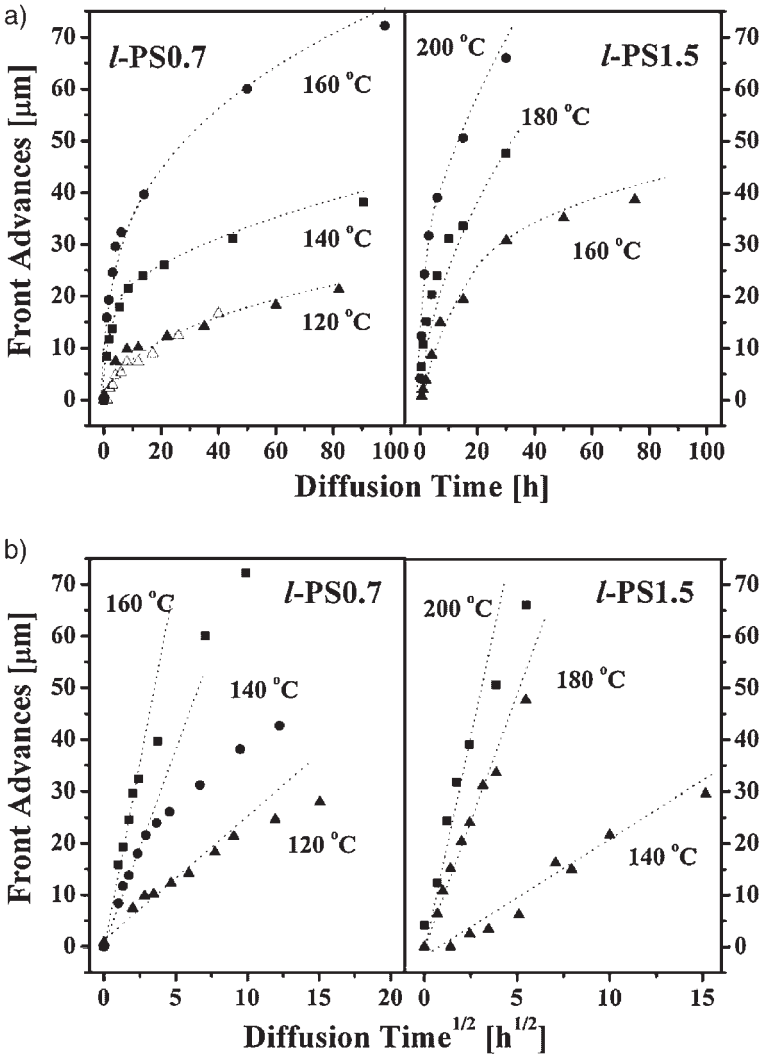

Figure 5. Plots of PS front advances vs. diffusion time at various temperatures for the *l*-PS0.7/PPO and *l*-PS1.5/PPO systems. (a) Linear plot and (b) Fickian fashion. The dotted lines have been drawn for eye guide.

Macromol. Chem. Phys. **2007**, *208*, 1110–1121

Macromolecular Journals
DOI: 10.1002/macp.200600658

glassy matrix does not give support for a case II mechanism, as one of the characteristic signatures of this mechanism is the linear propagation of the diffusion front with time, which originates in the coupling between diffusion and mechanical relaxation. One important fact, correctly pointed out by Nealey[11] but frequently ignored in the analyses made by other authors,[14,17,18] is the influence of the boundary conditions of the experiments on the time scaling laws. In limited-supply conditions, the liquid-PS volume fraction in the plateau region decreases with time and penetration depth. Therefore, the local driving force (osmotic suction or concentration gradients) changes continuously with time and depth. In contrast, under infinite supply of the liquid penetrant, a fully developed diffusion front propagates under a constant driving force with a constant velocity, because the properties of the plasticized layer remain fairly constant. Indeed, one may argue that the apparent nonlinearity observed in our experiments might arise from the limited supply of the liquid polymer. At this point, we also would have to consider the theoretical studies on case II diffusion carried out by Hui et al. and Argon et al. that show that at high penetrant concentrations, as in our case, the diffusion front velocity is relatively insensitive to changes in the concentration of the plasticized layer. To definitively clarify this issue, we are currently performing a series of experiments in which the same series of liquid penetrants are allowed to diffuse in a glassy matrix from an infinite source. We may say in advance that our first tests show the same time dependence than that reported here for limited supply conditions, with no indication of linear regime in the diffusion kinetics.

Figure 5(b) shows that the data scale relatively well with $t^{1/2}$, particularly in the *l*-PS1.5/PPO system. Notice the quite wide range of diffusion temperatures covered by our experiments, from 80 °C below to 35 °C above the matrix T_g. The deviation from the $t^{1/2}$ scaling in the form of downward curvature observed in all the experiments, more noticeable in the *l*-PS0.7/PPO system, can be explained in terms of changes in the diffusion coefficients as the diffusion process evolves. The transport of PPO molecules toward the liquid layer increases the local T_g along the PS diffusion path reducing the gap between the diffusion temperature and the local T_g. The effect is more pronounced in the *l*-PS0.7/PPO system due to the wider range of T-T_g covered by the experiment. All these features are typical of liquid-liquid diffusion between components with different T_g and we will see that all of them are quantitatively predicted by a diffusion model based on liquid polymer dynamics and Williams-Landel-Ferry (WLF) scaling. A similar time scaling was reported by Kramer et al. in their diffusion experiments with high molecular weight liquid PS, carried out at 5–40 °C below the matrix T_g.[23] Results published by Lin on a similar system show, for some of the data, interface displacements at constant velocity for short diffusion times that evolves toward a $t^{1/2}$ scaling for longer diffusion times.[14]

Osmotic Suctions and Activation Energies

The central feature of the case II mechanism is its rate-limiting step controlled by the mechanical relaxation of the solid polymer. A rigorous description of the mechanics and thermodynamics involved in the controlling step has been recently given by Argon.[10] The driving force for small molecules penetration, referred by Argon as "osmotic suction" (Σ), arises from the differences in its concentration with respect to its equilibrium value and it is defined in the context of the thermodynamics of osmosis as

$$\Sigma = \frac{RT}{\Omega} \ln\left(\frac{\Phi_{eq}}{\Phi}\right) \quad (1)$$

where Ω is the partial molar volume of the penetrant, Φ the concentration of penetrant at a given place, and Φ_{eq} its temperature-dependent value at equilibrium. When the liquid penetrant, driven by Σ, diffuses into the glassy matrix, it creates a dilatational misfit. This sets up a biaxial stress field, which has deviatory and pressure components, both of which increase in the direction of increasing liquid penetrant concentration.[10] The pressure component acts counteracting the osmotic suction, while the deviatory component will eventually bring the originally glassy polymer toward a generalized plastic yield. Case-II diffusion takes place when the osmotic suction overcomes the misfit-induced pressure, and, at the same time, the deviatory-induced stress overcomes the matrix yield stress. In this situation, the polymer just ahead of the moving front is swollen and this swelling rate controls further penetration of the small molecules.

High values of osmotic suction are thus a key factor to trigger a diffusion mechanism controlled by case II. The values of osmotic suction defined in Equation (1) depend inversely on the molar volume of the penetrant molecule Ω, which in turn can be expressed as M/δ, where M is the penetrant molecular weight and δ its density. For example, compared at the same composition gradients, the liquid polymers used by Lin and coworkers (PS with $\overline{M}_n$ from 9 to 2 000 $kg \cdot mol^{-1}$, $\delta \approx 1.05$ $g \cdot mL^{-1}$), produce osmotic suctions between 100 and 20 000 times smaller than that exerted by a small molecule such as toluene ($M = 92$ $g \cdot mol^{-1}$, $\delta \approx 0.87$ $g \cdot mL^{-1}$). Those values are between 200 and 40 000 times smaller than the osmotic suction associated with the methanol ($M = 32$ $g \cdot mol^{-1}$, $\delta \approx 0.79$ $g \cdot mL^{-1}$) used in the experiments of Thomas and Windle.

Clearly, large molecules as liquid polymers generate osmotic suction orders of magnitude smaller than those produced by small-sized penetrants in systems where case II has been effectively verified.

Although a substantial amount of work have been focused on its diffusion kinetics, another remarkable but less emphasized feature of case II is its temperature dependence, characterized by values of activation energies that reflect the process of plastic deformation of the glassy polymer that takes place at the diffusion front. This aspect has been addressed by Kramer,[25] and more recently by Durning.[26] One of the predictions of Thomas and Windle's model is that the apparent activation energy for the diffusion front advance (E_{df}) is a combination of the activation energy for diffusion in the glass (E_D) and for plastic flow of the glassy polymer at zero penetrant concentration (E_η):

$$E_{df} = \frac{E_\eta + E_D}{2} \tag{2}$$

Kramer demonstrated conclusively this relationship by measuring independently E_D from data of diffusion coefficients characterizing the Fickian precursors, E_η from simple creep test, and E_{df} from the advancing front kinetics in case II conditions. On the other hand, Vrentas developed an elaborated description of the relationship between E_D and E_η in the framework of the free volume theory for small penetrant-polymer diffusion.[27] Following Vrentas, E_D and E_η are related through ξ, the ratio of the critical molar volume of the penetrant jumping unit (V_s) to that of the so-called polymeric jumping unit (V_0):

$$E_D = \xi E_\eta \tag{3}$$

V_0 can be seen as the volume of polymer segments that have to move cooperatively for the transport process to occur. In the free-volume interpretation ξ depends mainly on the architecture of the monomer units and penetrant. For typical small penetrant-glassy polymer systems, the penetrant needs a smaller volume to complete a jump than does a polymeric jumping unit and $\xi < 1$.[28] As a consequence, the E_η contribution dominates over E_D. The free-volume theory has been verified by the extensive work of Vrentas and it has been recently confirmed in the context of case II by Durning et al.[29]

Figure 6 shows an Arrhenius plot of instantaneous front velocity (V_{df}) obtained from the analysis of our Raman data. Instantaneous velocities were calculated from the derivative of the front advances versus time plot as detailed elsewhere.[11,13] To focus only on the effect of temperature, each set of data correspond to similar stages in the diffusion process as they were calculated at the same value of liquid-polymer concentration at the plateau region (Φ_{pl}) and from experiments involving similar initial thicknesses for the low-T_g layer (60–70 μm). The solid symbols correspond to data of the *l*-PS0.7/PPO system, with V_{df} values calculated at two stages of the diffusion process, $\Phi_{pl} = 0.6$ (triangles) and $\Phi_{pl} = 0.5$ (circles). The open symbols refer to the *l*-PS1.5/PPO pair and they were calculated at $\Phi_{pl} = 0.7$.

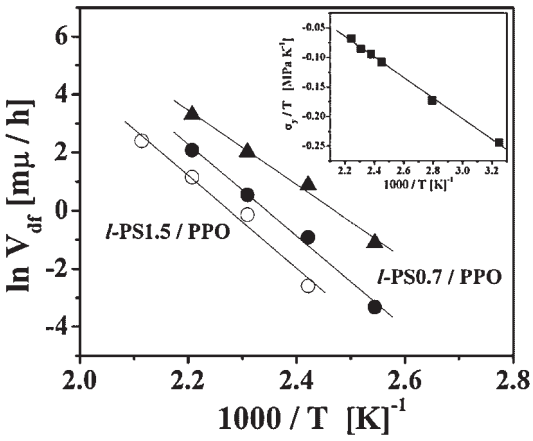

Figure 6. Arrhenius plot of ln(V_{df}) against 1/T over the temperature range from $T_g = -80$ to $+20$. Solid symbols: *l*-PS0.7/PPO at $\Phi_{pl} = 0.6$ (triangles) and at $\Phi_{pl} = 0.5$ (circles). Open symbols: *l*-PS1.5/PPO at $\Phi_{pl} = 0.7$. The lines represent the linear fittings used to calculate E_{df}. The inset shows the data taken from Creton's work plotted in Eyring fashion.

The data yield apparent activation energies for polymer diffusion (E_{df}) of 31.3 ± 0.9 kcal · mol^{-1} ($\Phi_{pl} = 0.5$) and 25.5 ± 0.9 kcal · mol^{-1} ($\Phi_{pl} = 0.6$) for the *l*-PS0.7/PPO pair over the temperature range of 120–180 °C. From the *l*-PS1.5/PPO data, we obtained $E_{df} = 31.7 \pm 1.6$ kcal · mol^{-1} at $\Phi_{pl} = 0.7$ in the range of 140–200 °C. The lower value of E_{df} obtained at earlier stages on the diffusion process ($\Phi_{pl} = 0.6$) in the *l*-PS0.7/PPO system, indicates that the temperature interval between the experimental temperature and the local T_g at the controlling step plays a role, as predicted by the WLF equation. At $\Phi_{pl} = 0.6$, the T_g of the plasticized layer (38 °C), is about 20 °C lower than that corresponding at $\Phi_{pl} = 0.5$, as measured by DSC. Consistently, the E_{df} values obtained are almost coincident in experiments where the difference between the experimental temperature and the average T_g at the plateau region are comparable (*l*-PS1.5/PPO at $\Phi_{pl} = 0.7$ and for *l*-PS1.5/PPO at $\Phi_{pl} = 0.6$). Also notice that T_g at the plateau region in the *l*-PS1.5/PPO pair at $\Phi_{pl} = 0.7$ is about 18 °C higher than that of the *l*-PS0.7/PPO pair at $\Phi_{pl} = 0.5$, nearly the same value that the shift in the temperature interval over which E_{df} is averaged (20 °C).

The values of E_{df} can be compared with the activation energy for plastic flow in the glassy solid matrix, E_η, expected to control case II. We obtained E_η from the

Macromol. Chem. Phys. **2007**, *208*, 1110–1121

Macromolecular Journals

DOI: 10.1002/macp.200600658

extensive measurements of plasticity as a function of temperature on the PS-PPO polymer pair and its blends carried out by Creton et al.[30] The authors obtained yield stresses (σ_y) from compression test at temperatures below T_g, for various temperatures and blend compositions (see Figure 6 of ref.[30]). In the inset of our Figure 6, we have plot data taken from Creton's work in Eyring fashion (σ_y/T vs. $1/T$). We chose the data corresponding to pure PPO, a close approximation to the composition of our matrices, in a temperature interval between 15 and 150 °C below T_g, which covers quite well that of our experiments. In the Eyring view, the slope of this plot yields E_η. From the corresponding linear regression of the Creton's data we obtained $E_\eta = 55$ kcal · mol^{-1}. The Eyring analysis also yields the so-called activation volume, which represents the volume of polymer segments which have to move cooperatively for the plastic deformation to occur. Notice that the activation volume is analogous to the previously defined V_0. Creton reported data for the activation volume that, despite a moderate dependence on composition, are on the same order for both PS and PPO, about 1 nm^3 per molecule. In the context of the Vrentas analysis, these results yield values of ξ in the order of 1. Consequently, E_D and E_η should be comparable in the PS-PPO system, with E_{df} values very close to that one would obtain for E_η.

Clearly, the values we obtained for E_{df} (25–30 kcal · mol^{-1}) are much lower than those expected for a diffusion mechanism controlled by case II (nearly 55 kcal · mol^{-1}). In fact, one of the characteristic signatures of case II is the large value of activation energy that characterizes the process, much higher than those observed in Fickian diffusion. In this sense, the values obtained are consistent with the Fickian character observed in the time scaling laws of the diffusion kinetics. In the next section, we will show that the temperature dependency of the process is well predicted by the WLF equation.

Modeling of the Diffusion Profiles and Diffusion Kinetics

We end the paper comparing the experimental results obtained with the predictions of a model for liquid-liquid polymer diffusion. The model describes the Fickian diffusion between two liquid polymers with different viscosity, through the use of a variable diffusion coefficient.[3] To account for the dissimilar diffusivities of the components a bulk flow contribution is included in the transport equations. Full details of the model formulation and the parameters used for the numerical simulations for the PS-PPO system have been published in earlier work.[19] Briefly, the flux of individual components is expressed in terms of the Onsager formalism as the product of a thermodynamic factor, related to the individual gradients of chemical potential, and a kinetic factor, associated with the mobilities of each component. The thermodynamic factor is derived from the Flory-Huggins theory and it is expressed as a function of distributions of molecular weights for each component and the Flory-Huggins interaction parameter of the system. The kinetic factor is in turn expressed in terms of the monomeric friction coefficients of each component as a function of blend composition, assuming a suitable diffusion dynamics (i.e., Rouse, reptation).[4] Changes in the monomeric friction coefficients with free volume are calculated with the WLF equation, using the local T_g as reference temperature. As the PS-PPO blends behave in thermorheological simple fashion, the same WLF scaling can be used to describe the dynamics of both PS and PPO species for any blend composition.[4] The reference temperature is adjusted point-by-point along the diffusion coordinate as a function of the local blend composition. The variations of blend T_g as a function of PS composition were determined independently for the three systems studied from DSC experiments on PS-PPO blends prepared by freeze-drying. The experimental T_g values fit well to a third-degree polynomial, whose coefficients for the three systems studied are shown in Table 2. These analytical expressions were used to calculate local T_g values as a function of blend composition in computer simulations.

The model allows the calculation of PS concentration profiles as a function of PS molecular weight, diffusion temperature, and annealing time. The PS molecular weight enters in the calculation through the thermodynamic and kinetics factor and, indirectly, through variations in local T_g with blend composition; for further details see ref.[19]. In the kinetics factor, Rouse-type dynamics was assumed for all the liquid-PS components.

To avoid the convolution step between model predictions and instrumental broadening, needed to properly interpret raw data from depth-profiling experiments,[19] we directly compare the computer simulations with the data obtained by surface analysis, virtually free of instrumental artifacts. Experimental and calculated PS concentration profiles are compared in Figure 2(a)–2(c), where model calculations have been represented as solid lines. One can see that for all the cases the model reproduce with

Table 2. Polynomial coefficients used to fit the experimental data of blend T_g obtained by DSC as a function of PS volume fraction (Φ^{PS}). The polynomial form used was $T_g(\Phi^{PS}) = A + B\Phi^{PS} + C(\Phi^{PS})^2 + D(\Phi^{PS})^3$.

System	*A*	*B*	*C*	*D*
l-PS0.7/PPO	483.7	−412.3	206.7	–
l-PS1.5/PPO	481.0	−297.0	180.3	−49.2
l-PS3.9/PPO	479.8	−276.3	223.28	−80.0

remarkable precision all the features of the profiles, predicting flat curves in regions of low viscosity (PS-rich) and a much steeper slope when approaching to the solid matrix (PPO-rich layer). The marked asymmetry in the predicted concentration profiles originates in the dramatic changes of the monomeric friction coefficient values along the diffusion coordinate, in turn controlled by the local T_g through the WLF scaling, as extensively discussed in our previous work.[13]

The predicted kinetics of the diffusion fronts are compared with experimental data through Figure 3(a)–3(b). To calculate front advances from the calculated profiles, we used the PS concentration at the plateau region and the area under the profile, the same methodology employed to obtain the front advances from the experimental data. The model predicts precisely the evolution of the diffusion process at 160 °C for any of the molecular weights and for the complete range of annealing times. Subtle features of the process, such as the downward curvature in the front advances observed in Figure 3(b), are also correctly predicted. The same agreement was found for the rest of temperatures studied. A consequence of this good agreement, particularly the response to temperature, indicates that the WLF scaling effectively predicts the temperature dependency of the diffusion process. As suggested in previous work,[31] it indicates that the controlling step of the diffusion process is placed at the liquid polymer-matrix interphase, at liquid polymers concentrations corresponding to a local T_g quite lower than the annealing temperatures.

Conclusion

Relevant aspects of the diffusion mechanism in the liquid/solid PS/PPO polymer pair have been examined through extensive diffusion experiments carried out at temperatures well below the T_g of the solid polymer on a series of low-molecular weight PS samples. No signatures of the linear regime characteristic of case II were observed despite the fact that the osmotic suctions associated with the liquid polymers employed are expected to be much larger than those generated by the high molecular weight counterparts and that the range of temperatures covered by the experiments are the widest studied ever for this polymer pair. On the other hand, the fact that a model developed for liquid–liquid polymer diffusion fully describes all the diffusion experiments suggests a diffusion control mechanism with Fickian character.

From our experiments, we infer that the liquid molecular weight appears affecting the diffusion rates through free volume effects, well accounted by the diffusion model based on liquid dynamics and WLF scaling used to reproduce the experiments. The way that temperature operates on the diffusion process and the E_{df} values found are consistent with these observations confirming the liquid characteristics of the diffusion controlling step. This aspect of the problem has been overlooked in previous studies of liquid–glassy polymer diffusion, more focused in the diffusion kinetics or on the shape of the diffusion profiles, despite the fact that the analysis of the temperature dependence directly reflects the nature of the rate-controlling step of the process.

In recent works, we postulated the idea that because of the negligible osmotic suctions generated at the interface and the low diffusion coefficients associated with large liquid molecules, the conditions for case II cannot be met at liquid/glassy polymer interphases. The results of this work can be taken as another piece of evidence that further supports this view.

Acknowledgements: The authors thank *ANPCyT* (PICT 03-12-14570) for supporting this research.

Received: December 19, 2006; Revised: March 5, 2007; Accepted: March 5, 2007; DOI: 10.1002/macp.200600658

Keywords: calculations; case-II diffusion; confocal Raman microspectroscopy; glassy polymer matrices; melt; polymer diffusion

[1] J. D. Ferry, "*Viscoelastic Properties of Polymers*", Wiley, New York 1980.
[2] P. G. de Gennes, *J. Chem. Phys.* **1971**, *55*, 572.
[3] E. J. Kramer, P. F. Green, C. J. Palmstrom, *Polymer* **1984**, *25*, 473.
[4] R. J. Composto, E. J. Kramer, D. M. White, *Polymer* **1990**, *31*, 2320.
[5] [5a] P. F. Green, *Macromolecules* **1991**, *24*, 3373; [5b] P. F. Green, D. B. Adolf, L. Gilliom, *Macromolecules* **1991**, *24*, 3377.
[6] R. H. Colby, *Polymer* **1989**, *30*, 1275.
[7] [7a] N. L. Thomas, A. H. Windle, *Polymer* **1980**, *21*, 613; [7b] N. L. Thomas, A. H. Windle, *Polymer* **1981**, *22*, 627; [7c] N. L. Thomas, A. H. Windle, *Polymer* **1982**, *23*, 529.
[8] [8a] C.-Y. Hui, K.-C. Wu, R. C. Lasky, E. J. Kramer, *J. Appl. Phys.* **1987**, *61*, 5129; [8b] C.-Y. Hui, K.-C. Wu, R. C. Lasky, E. J. Kramer, *J. Appl. Phys.* **1987**, *61*, 5137.
[9] [9a] R. C. Lasky, E. J. Kramer, C.-Y. Hui, *Polymer* **1988**, *29*, 673; [9b] T. P. Gall, R. C. Lasky, E. J. Kramer, *Polymer* **1990**, *31*, 1491; [9c] T. P. Gall, E. J. Kramer, *Polymer* **1991**, *32*, 265.
[10] A. S. Argon, R. E. Cohen, A. C. Patel, *Polymer* **1999**, *40*, 6991.
[11] P. F. Nealey, R. E. Cohen, A. S. Argon, *Polymer* **1995**, *36*, 3687.
[12] Y. Feng, R. A. Weiss, A. Karim, C. C. Han, J. F. Anker, H. Kaiser, D. G. Peiffer, *Macromolecules* **1996**, *29*, 3918.
[13] J. P. Tomba, J. M. Carella, D. García, J. M. Pastor, *Macromolecules* **2001**, *34*, 2277.
[14] C. J. Lin, I. F. Tsai, C. M. Yang, M. S. Hsu, Y. C. Ling, *Macromolecules* **2003**, *36*, 2464.
[15] M. Geoghegan, R. A. L. Jones, M. G. D. Van der Grinten, A. S. Clough, *Polymer* **1999**, *40*, 2323.
[16] J. P. Tomba, J. M. Carella, J. M. Pastor, *Macromolecules* **2005**, *38*, 4355.

DOI: 10.1002/macp.200600658

[17] B. B. Sauer, D. J. Walsh, *Macromolecules* **1991**, *24*, 5948.
[18] E. Jabbari, N. A. Peppas, *Macromolecules* **1993**, *26*, 6229.
[19] J. P. Tomba, J. M. Carella, J. M. Pastor, J. C. Merino, *Polymer* **2002**, *43*, 6751.
[20] N. J. Everall, *Appl. Spectrosc.* **2000**, *54*, 773.
[21] J. P. Tomba, J. M. Carella, J. M. Pastor, *Appl. Spectrosc.* **2006**, *54*, 1515.
[22] J. P. Tomba, E. de la Puente, J. M. Pastor, *J. Polym. Sci.; Part B: Polym. Phys.* **2000**, *38*, 1013.
[23] R. J. Composto, E. J. Kramer, *J. Mater. Sci.* **1991**, *26*, 2815.
[24] [24a] J. Barrales-Rienda, D. Pepper, *J. Polym. Sci.; Polym. Lett. Ed.* **1966**, *4*, 939; [24b] P. J. Akers, G. Allen, M. J. Bethell, *Polymer* **1968**, *9*, 575.
[25] R. C. Lasky, E. J. Kramer, C.-Y. Hui, *Polymer* **1988**, *29*, 1131.
[26] M. M. Hassan, C. J. Durning, *J. Polym. Sci. ; Part B: Polym. Phys.* **1999**, *37*, 3159.
[27] J. S. Vrentas, *J. Appl. Polym. Sci.* **1978**, *22*, 2325.
[28] J. S. Vrentas, *J. Polym. Sci. ; Polym. Phys. Ed.* **1979**, *17*, 1085.
[29] C. J. Durning, M. M. Hassan, H. M. Tong, K. W. Lee, *Macromolecules* **1995**, *28*, 4234.
[30] C. Creton, J.-L. Halary, L. Monnerie, *Polymer* **1998**, *40*, 199.
[31] L. M. Arzondo, J. P. Tomba, J. M. Carella, J. M. Pastor, *Macromol. Rapid Commun.* **2005**, *26*, 632.